

Chemically-induced swelling of hydrogels

John Dolbow,[†] Eliot Fried,[‡] Huidi Ji[†]

[†]Department of Civil and Environmental Engineering
Duke University
Durham, NC 27708-0287, USA

[‡]Department of Mechanical Engineering
Washington University in St. Louis
St. Louis, MO 63130-4899, USA

Abstract

We consider a continuum model for chemically-induced volume transitions in hydrogels. Consistent with experimental observations, the theory allows for a sharp interface separating swelled and collapsed phases of the underlying polymer network. The polymer chains are treated as a solute with an associated diffusion potential and their concentration is assumed to be discontinuous across the interface. In addition to the standard bulk and interfacial equations imposing force balance and solute balance, the model involves a supplemental interfacial equation imposing configurational force balance. We present a hybrid eXtended-Finite-Element/Level-Set Method (XFE/LSM) for obtaining approximate solutions to the governing equations of the model. As an application, we consider the swelling of a spherical specimen whose boundary is traction-free and is in contact with a reservoir of uniform chemical potential. Our numerical results exhibit good qualitative comparison with experimental observations and predict characteristic swelling times that are proportional to the square of the specimen radius. Our results also suggest several possible synthetic pathways that might be pursued to engineer hydrogels with optimal response times.

Keywords: A. Hydrogels; A. Phase transitions; A. Chemo-mechanical process; B. Configurational forces; B. Sharp interface

1 Introduction

Stimulus responsive hydrogels are crosslinked, macromolecular polymer networks immersed in a solvent, synthesized to exhibit large volumetric swelling in response to a variety of environmental stimuli. Importantly, hydrogels may act as both sensors and switches. When combined with the lack of a need for an external power source, this multifunctionality suggests a broad spectrum of applications. For example, hydrogels have recently been designed to serve as drug carriers/pumps in the bloodstream for therapeutic biomedical applications (Eichenbaum et al, 1999) and as microfluidic actuators (Beebe et al, 2000). But a lack of understanding of the relationship between gel composition and response kinetics has hindered the design of these materials and, accordingly, delayed the transfer of new applications from the laboratory to the marketplace. In this paper, we present a new theory for the chemo-mechanical response of hydrogels and demonstrate its predictive capabilities with the aid of advanced numerical methods.

For particular hydrogel compositions and external environmental conditions, a phase interface develops and the motion of this interface corresponds with the swelling response of the gel. The transition from a distinct collapsed phase to a swollen phase with the

evolution of the interface was first observed by Tanaka (1978) for polyacrylamide-based hydrogels. The phenomenon is often referred to as a “volume transition” (Dušek, 1993) and a similar type of behavior has been observed by Budtova and Navard (1998) for polyelectrolyte gels in saline solutions. More recently, Olsen et al. (2000) developed a particle-imaging technique to observe the evolution of such hydrogel “microstructures.” The importance of understanding this phenomenon rests on the fact that the kinetic response of hydrogels is directly coupled to the motion of the phase interface. Moreover, understanding the chemo-mechanical interaction between distinct phases facilitates the design of new hydrogels with specific drug release characteristics (Budtova, 1998).

In addition to the distinct phase transition exhibited by hydrogels, recent attention has focused on the “ripple” patterns observed on the surface of gel specimens during sufficiently large volumetric swelling or shrinking (Tanaka et al, 1987). The surface instability is initiated at the microscale, and the size of the associated cusps on the surface can expand to the characteristic size of the specimen itself. Indeed, rather dramatic changes in surface pattern have recently been observed on *N*-isopropylacrylamide (NIPA) gels as a function of temperature drift rate or superheating (Bai and Suzuki, 2000). These phenomena seem to mandate the need for models that account for curvature effects during the swelling process and, in addition, for the possibility of cusp formation.

A significant number of phenomenological and empirical models have been developed to describe the swelling of hydrogels; a review of many of these can be found in Onuki (1993). With regard to representing the transition dynamics for multi-phase gels separated by a sharp interface, however, only a limited amount of previous research can be identified. Tomari and Doi (1994) developed a one-dimensional model that correlates with the experimental result of swelling times proportional to the square of gel radius. This model was later extended to the spherically symmetric case by Tomari and Doi (1995), where the authors employed a Flory–Huggins type free-energy functional for ionic gels in a neutral solution. For pH-sensitive gels, Gehrke et al. (1992) adopted a classical shrinking core model to cylindrical configurations and correlated their results to experimental measurements of the motion of the sharp ionization front. Their model did not consider large volume changes and the diffusion coefficients obtained from the correlation process were found to be significantly lower than those reported elsewhere.

In the majority of the works cited above, the “collective diffusion” assumption proposed by Tanaka et al. (1973) was invoked. Collective diffusion assumes that swelling occurs simultaneously throughout the medium. Under this assumption, the characteristic time of swelling is incorporated by modifying the force balance to consider the “frictional force” acting between the polymer network and the solvent. This yields a parabolic governing equation that, indeed, predicts collective diffusion. Swelling times obtained using this approach do correlate reasonably well with experimental results. However, in contrast with the assumptions underlying this approach, the observations of Olsen et al. (2000) show clearly that swelling proceeds with the propagation of interfaces separating swelled and collapsed phases.

To model the roles of deformation, mass transport, and interface propagation in the chemo-mechanical swelling of hydrogels, we use an extension of the sharp-interface theory of Gurtin and Voorhees (1993) that accounts for finite strain. This theory of Gurtin and Voorhees (1993) is developed from the perspective of Gibbs (1878), who modeled phase interfaces as surfaces across which the material properties of the bulk phases may suffer discontinuities and, to account for localized interactions between phases, endowed these surfaces with excess fields. Of key importance in the theory is an interfacial equation, expressing configurational force balance (Gurtin and Struthers, 1990; Gurtin, 1995; Gurtin, 2000), which generalizes the Gibbs–Thomson relation arising in descriptions of alloy solidification (cf., e.g., Mullins and Sekerka (1963)) and supplements the conven-

tional equations which express standard force balance and mass balance in the bulk phases and across the interface.

A number of alternative strategies have been advocated for the construction of approximate numerical solutions to problems arising in sharp-interface models for phase transitions. As it is not our intention to provide a comprehensive account of these methods, we refer the reader to the recent review of Udaykumar et al. (1999). The main point is that optimal rates of convergence in suitable error norms can be obtained for these problems only if the numerical approximation retains the sharp interface representation. Within the context of finite-element approximations, this result imposes overly restrictive conditions on the mesh. Until recently, one of the few strategies for capturing the local discontinuities near an evolving sharp interface was to adopt moving-mesh formulations akin to those developed in the pioneering work of Lynch and O’Neill (1981). Among the many concerns with such formulations is the potential for severe mesh distortion, especially in two- and three-dimensional problems where the geometry of the interface is generally non-planar.

The eXtended-Finite-Element Method (X-FEM) (Moës et al, 1999; Dolbow, 1999) is a variation on the partition-of-unity framework (Melenk and Babuška, 1996) for building local, non-polynomial ansatz spaces into an approximation. A further variation on this theme concerns the eXtended-Finite-Element/Level-Set Method (XFE/LSM), wherein both the local solution and geometry of arbitrarily evolving features are represented with evolving functions. The coupling of the two methods was first conceived in Sukumar et al. (2001), albeit for stationary geometric features. Recently, the XFE/LSM has been employed to simulate phase transition problems where the interface is assumed to be sharp. Merle and Dolbow (2002) developed a one-dimensional formulation for Stefan problems and Ji et al. (2002) recently generalized this approach to multi-dimensional solidification problems.

In this paper, the basic techniques of the XFE/LSM are extended to account for the finite strains associated with the extreme ($\sim 1000\%$) volumetric change possible in hydrogels. Central to our approach is the use of discontinuous enrichment functions to capture discontinuities in the gradients of the deformation and the diffusion potential across the phase interface. Lagrange multipliers are employed to satisfy additional constraints at the interface and the multipliers are subsequently used to interpret the pertinent flux quantities. This allows for the accurate simulation of the evolution of the phase interface without recourse to remeshing or moving mesh techniques. It is also qualitatively different from previous numerical strategies (Tomari and Doi, 1994; Tomari and Doi, 1995), strategies wherein the interface is smeared over a single element. While our particular approach does share common features with recent works for simulating the thermal oxidation of silicon (Rao et al, 2000; Garikipati and Rao, 2001), it also bears a number of distinctions which are elucidated more fully in this document.

As an elementary application of the theory presented here, we consider the case of a spherical specimen subjected to purely radial chemo-mechanical boundary conditions. In particular, the boundary of the specimen is assumed to be traction free and in contact with a solvent-rich reservoir within which the diffusion potential is spatially uniform but may vary in time. We seek solutions in which the deformation and diffusion potential are assumed to be radially symmetric. This leads to a nonlinear initial-boundary-value problem which we solve numerically using the XFE/LSM.

This paper is organized as follows. In Section 2, we present the governing equations. In Section 3, we describe the variational form of a generic mixed boundary-value problem and the discretization with the XFE/LSM. In Section 4, we consider a spherically symmetric specimen subjected to purely radial loadings and provide the numerical results obtained by our algorithm. Finally, a summary of our results and discussion of future

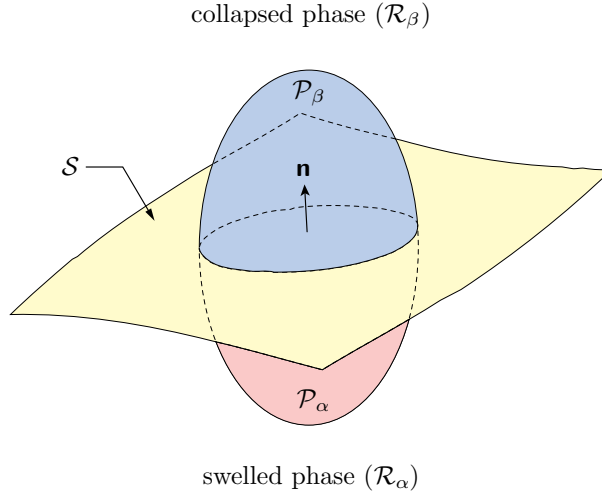


Figure 1: Schematic indicating: the regions occupied by the swelled and collapsed phases; the evolving interface \mathcal{S} , with unit normal \mathbf{n} directed into the collapsed phase; a fixed control volume \mathcal{P} divided by \mathcal{S} into time-dependent regions \mathcal{P}_α and \mathcal{P}_β in the swelled and collapsed phases.

directions are provided in Section 6.

2 Governing equations

To account for the roles of deformation, mass transport, and interface propagation in the chemo-mechanical swelling of hydrogels, we work with an extension of the sharp-interface theory of Gurtin and Voorhees (1993) that accounts for finite strain.

We label the swelled and collapsed phases by α and β and write \mathcal{S} for the interface, which we take to divide the region \mathcal{R} occupied by the body into complementary subregions $\mathcal{R}_\alpha(t)$ and $\mathcal{R}_\beta(t)$. We write \mathbf{n} for the unit normal on \mathcal{S} , directed outward from \mathcal{R}_α as shown in Figure 1, and v for the (scalar) normal velocity of \mathcal{S} in the direction of \mathbf{n} .

Aside from the configuration of \mathcal{S} , the primary unknowns of the theory are deformation \mathbf{y} of the polymer network and the diffusion potential u of the polymer chains. Of basic importance are the assumptions of coherence

$$[[\mathbf{y}]] = \mathbf{0}, \quad (2.1)$$

and local chemical equilibrium

$$[[u]] = 0, \quad (2.2)$$

where $[[g]] = \overset{+}{g} - \bar{g}$, with $\overset{+}{g}$ the interfacial limit of a bulk field g from within the collapsed phase and \bar{g} the corresponding limit from within the swelled phase.

We neglect inertia and external forces. In addition, motivated by the experimental observations of Gehrke et al. (1992), we restrict attention to processes where the time scale associated with the motion of the interface (i.e., volume transitions) is slow compared to bulk diffusion. Then, the bulk equations expressing deformational force balance on

solute balance on phase- γ are

$$\left. \begin{aligned} \text{Div} \left(\frac{\partial W_\gamma(\mathbf{F})}{\partial \mathbf{F}} \right) &= \mathbf{0}, \\ m_\gamma \text{Div}(\text{Grad } u) &= 0, \end{aligned} \right\} \quad (2.3)$$

where $\mathbf{F} = \text{Grad } \mathbf{y}$ is the deformation gradient, W_γ is the strain-energy function of phase- γ (which in keeping with invariance can be expressed as a function of the scalar invariants of $\mathbf{F}\mathbf{F}^\top$), and $m_\gamma > 0$ is the constant mobility of polymer chains in phase- γ . Further, the equations expressing deformational force balance, solute balance, and normal configurational force balance (which is a generalization, appropriate to the present context, of the Gibbs–Thomson relation arising in theories of alloy solidification) on the interface are

$$\left. \begin{aligned} \left[\left[\frac{\partial W_\gamma(\mathbf{F})}{\partial \mathbf{F}} \right] \right] \mathbf{n} &= \mathbf{0}, \\ [c_\gamma] \nu + [m_\gamma \text{Grad } u] \cdot \mathbf{n} &= 0, \\ [c_\gamma] \mathbf{u} = \sigma \mathbf{K} + \mathbf{n} \cdot \left[\left[W_\gamma(\mathbf{F}) \mathbf{I} - \mathbf{F}^\top \frac{\partial W_\gamma(\mathbf{F})}{\partial \mathbf{F}} \right] \right] \mathbf{n}, \end{aligned} \right\} \quad (2.4)$$

where c_γ is the constant concentration of polymer chains in phase- γ , $\mathbf{u} = u|_{\mathcal{S}}$ is the interfacial diffusion potential, σ is the interfacial tension, and $K = -\text{Div}_{\mathcal{S}} \mathbf{n}$ is (twice) the interfacial mean curvature.

We emphasize that the only explicit coupling between the fields \mathbf{y} and u evident from (2.3) and (2.4) is through the normal configurational balance (2.4)₃.

The bulk and interfacial equations (2.3) and (2.4) provide a phenomenological model for the study of chemically-induced volume transitions in hydrogels. A more general description would involve the provision, for each phase, of a Gibbs free-energy density encompassing interactions between network distortion and chemistry. Ideally, the form of these densities would be determined by microphysical considerations. Similar comments apply to the mobilities, which are the key kinetic ingredients of the theory. As opposed to taking these to be constants, it would be preferable to allow for dependence of these quantities on network distortion and chemistry, as guided by molecular arguments.

3 Numerical approximation

Here, we use the hybrid eXtended-Finite-Element/Level-Set Method (XFE/LSM) to discretize the bulk and interfacial equations (2.3) and (2.4), while enforcing the conditions (2.1) and (2.2) of coherency and local chemical equilibrium. Our approach follows upon work of Merle and Dolbow (2002) and Ji et al. (2002) (see Dolbow (1999) for additional details). We begin by deriving an equivalent variational formulation of the governing equations. We then construct an enhanced approximation space for capturing gradient discontinuities across the phase interface. We conclude with a discussion of the solution strategy for the coupled systems of equations.

3.1 Variational formulation

In addition to the bulk and interfacial equations presented in Section 2, we require boundary conditions. Writing $\boldsymbol{\nu}$ for the unit orientation of $\partial \mathcal{R}$, directed outward from \mathcal{R} , we assume that

$$\mathbf{y}|_{(\partial \mathcal{R})_m} = \boldsymbol{\eta} \quad \text{and} \quad (\mathbf{S}\boldsymbol{\nu})|_{(\partial \mathcal{R})_t} = \mathbf{s}, \quad (3.1)$$

with $(\partial\mathcal{R})_m$ and $(\partial\mathcal{R})_t$ complementary subsets of $\partial\mathcal{R}$, and that

$$u|_{(\partial\mathcal{R})_p} = v \quad \text{and} \quad (\mathbf{h} \cdot \boldsymbol{\nu})|_{(\partial\mathcal{R})_f} = h, \quad (3.2)$$

with $(\partial\mathcal{R})_p$ and $(\partial\mathcal{R})_f$ complementary subsets of $\partial\mathcal{R}$.

3.1.1 Weak statement of the deformational force balance and coherency

Our variational formulation is non-standard in that the coherency condition (2.1) is enforced weakly using a Lagrange multiplier \mathbf{p} . We begin by defining a functional

$$F(\mathbf{y}, \mathbf{p}) = \sum_{\gamma=\alpha,\beta} \int_{\mathcal{R}_\gamma} W_\gamma(\mathbf{F}) dv - \int_{(\partial\mathcal{R})_t} \mathbf{s} \cdot \mathbf{y} da - \int_S \mathbf{p} \cdot \llbracket \mathbf{y} \rrbracket da. \quad (3.3)$$

The bulk force balance (2.3)₁, the interfacial force balance (2.4)₁, the coherency condition (2.1), and the traction boundary condition (3.1)₂ follow on requiring that F be stationary.

We let \mathcal{A}_m and \mathcal{L}_m denote, respectively, the space of motions and that are sufficiently regular and comply with the Dirichlet conditions (3.1)₁ and the space of sufficiently regular Lagrange multipliers.¹ The requirement that F be stationary yields the variational boundary-value-problem: find \mathbf{y} in \mathcal{A}_m and all \mathbf{p} in \mathcal{L}_m such that

$$\left. \begin{aligned} \sum_{\gamma=\alpha,\beta} \int_{\mathcal{R}_\gamma} \frac{\partial W_\gamma(\mathbf{F})}{\partial \mathbf{F}} \cdot \text{Grad } \mathbf{w} dv &= \int_{(\partial\mathcal{R})_t} \mathbf{s} \cdot \mathbf{w} da + \int_S \mathbf{p} \cdot \llbracket \mathbf{w} \rrbracket da, \\ \int_S \mathbf{q} \cdot \llbracket \mathbf{y} \rrbracket da &= 0, \end{aligned} \right\} \quad (3.4)$$

for all variations \mathbf{w} of \mathbf{y} and \mathbf{q} of \mathbf{p} belonging to suitable spaces \mathcal{V}_m and \mathcal{L}_m .

3.1.2 Weak statement of bulk solute balance, interfacial configurational force balance, and local chemical equilibrium

Our next step is also nonstandard. Analogous to our variational treatment of the force balance, we enforce the condition (2.2) of local chemical equilibrium using a scalar-valued Lagrange multiplier k which may jump across the interface.² Furthermore, as opposed to formulating a weak statement that imposes the bulk and interfacial solute balances (2.3)₂ and (2.4)₂, we formulate a weak statement that imposes the bulk solute balance (2.3)₂, the interfacial configurational balance (2.4)₃, and the condition of local chemical equilibrium. We begin by defining a functional

$$G(u, p) = \sum_{\gamma=\alpha,\beta} \int_{\mathcal{R}_\gamma} \frac{1}{2} m_\gamma |\text{Grad } u|^2 dv - \int_{\partial\mathcal{R}_h} hu da + \int_S \llbracket k(\mathbf{u} - u) \rrbracket da. \quad (3.5)$$

The requirement that this functional be stationary implies satisfaction of the bulk solute balance (2.3)₂, requires that the interfacial limits \bar{u}^+ and \bar{u}^- of the diffusion potential coincide and be equal to \mathbf{u} , viz.,

$$\bar{u}^+ = \bar{u}^- = \mathbf{u}, \quad (3.6)$$

¹We consider a space of admissible motions that allows for discontinuities across \mathcal{S} , even though such discontinuities are not expected in the solution to the strong form of the boundary value problem. Such variational formulations are often termed *hybrid*.

²In practice, two independent Lagrange multipliers are employed and these are indeterminate away from the interface. For the sake of convenience, we refer to these here as separate limiting values of a single bulk field k .

and thus ensures satisfaction of the normal configurational force balance (2.4)₃ and the condition (2.2) of local chemical equilibrium, while providing identifications,

$$\overset{\pm}{k} = \frac{\overset{\pm}{\mathbf{v}}}{m_\gamma \text{Grad } u \cdot \mathbf{n}}, \quad (3.7)$$

of the interfacial limits of the Lagrange multiplier with the corresponding interfacial limits of the normal component of the solute flux.

We denote the spaces of sufficiently regular diffusion potentials and Lagrange multipliers by \mathcal{A}_p and \mathcal{L}_p . The requirement that G be stationary yields the variational boundary-value problem: find u in \mathcal{A}_p and k in \mathcal{L}_p such that

$$\left. \begin{aligned} \sum_{\gamma=\alpha,\beta} \int_{\mathcal{R}_\gamma} m_\gamma \text{Grad } u \cdot \text{Grad } w \, dv &= \int_{(\partial\mathcal{R})_f} hw \, da - \int_S \llbracket kw \rrbracket \, da, \\ \int_S \llbracket (u - u)l \rrbracket \, da &= 0, \end{aligned} \right\} \quad (3.8)$$

for all variations w of u and l of k belonging to suitable spaces \mathcal{V}_p and \mathcal{L}_p .

3.1.3 Interfacial solute balance. Level-set formulation

We have presented variational formulations that lead to weak restatements of all of the equations in (2.3) and (2.4) except the interfacial solute balance (2.4)₂. Relying on the expressions (3.7) determining the interfacial limits of the Lagrange multiplier k , we impose (2.4)₂ in the strong sense via

$$\llbracket c_\gamma \rrbracket \mathbf{v} = -\llbracket k \rrbracket. \quad (3.9)$$

We represent the interface as the zero level-set $\mathcal{S}(t) = \{\mathbf{x} : \zeta(\mathbf{x}, t) = 0\}$ of a function ζ and, following Osher and Sethian (1988), replace (3.9) with the evolution equation

$$\dot{\zeta} + v^e |\text{Grad } \zeta| = 0, \quad (3.10)$$

where the extension velocity v^e is constrained to obey

$$v^e|_{\zeta=0} = \mathbf{v} = -\frac{k}{\llbracket c_\gamma \rrbracket} \quad (3.11)$$

Further, we require that $\text{Grad } v^e \cdot \text{Grad } \zeta = 0$, which is both necessary and sufficient (Sethian, 1999) to ensure that ζ is the signed distance from the interface \mathcal{S} . Since ζ is defined throughout \mathcal{R} , (3.10) is an evolution equation over \mathcal{R} . Similarly, v^e is defined over the entire domain \mathcal{R} , whereas \mathbf{v} is only defined on the interface \mathcal{S} .

3.2 Discretization with the XFE/LSM

3.2.1 Approximation for the deformation \mathbf{y}

Finite-element computations entail the projection of the solution space \mathcal{A}_m and the associated space \mathcal{V}_m of variations onto finite-dimensional subspaces \mathcal{A}_m^h and \mathcal{V}_m^h , and similarly for the Lagrange multipliers. The Galerkin approximation of the variational boundary-value problem stated in Section 3.1.1 reads: find \mathbf{y}^h in \mathcal{A}_m^h and \mathbf{p}^h in \mathcal{L}_m^h such that

$$\left. \begin{aligned} \sum_{\gamma=\alpha,\beta} \int_{\mathcal{R}_\gamma} \frac{\partial W_\gamma(\mathbf{F}^h)}{\partial \mathbf{F}^h} \cdot \text{Grad } \mathbf{w}^h \, dv &= \int_{(\partial\mathcal{R})_t} \mathbf{s} \cdot \mathbf{w}^h \, da + \int_S \mathbf{p}^h \cdot \llbracket \mathbf{w}^h \rrbracket \, da, \\ \int_S \mathbf{q}^h \cdot \llbracket \mathbf{y}^h \rrbracket \, da &= 0, \end{aligned} \right\} \quad (3.12)$$

for all variations \mathbf{w}^h of \mathbf{y}^h and \mathbf{q}^h of \mathbf{p}^h belonging to \mathcal{V}_m^h and \mathcal{L}_m^h .

We use M to denote the total number of elements in the mesh and consider a regular finite-element-triangulation $\mathcal{Q}^h = \cup_{e=1}^M \mathcal{Q}_e$, with $\mathcal{Q}^h = \mathcal{R}$ but with element edges chosen, generally, to be independent of the interface geometry. Letting $P^j(\mathcal{Q}_e)$ denote the space of complete polynomials of order less than or equal to j over element \mathcal{Q}_e , we introduce

$$\{\phi_i \in C^0(\mathcal{Q}^h) : \phi_i|_{\mathcal{Q}_e} \in P^j(\mathcal{Q}_e)\}, \quad (3.13)$$

where ϕ_i , $i = 1, 2, \dots$, are the nodal shape functions. We next consider the set of overlapping subdomains $\{\omega_i\}$ defining the support of each nodal shape function and an enrichment function g that possesses desirable approximation properties in the vicinity of the interface. The approximation for the deformation is given by

$$\mathbf{y}^h(\mathbf{x}, t) = \underbrace{\sum_{i \in I} \mathbf{c}_i(t) \phi_i(\boldsymbol{\xi}(\mathbf{x}))}_{\text{classical approximation}} + \underbrace{\sum_{j \in J} \mathbf{e}_j(t) \phi_j(\boldsymbol{\xi}(\mathbf{x})) g(\mathbf{x}, t)}_{\text{enrichment}} \quad (3.14)$$

where $\boldsymbol{\xi}$ are the local element coordinates. In the above, I denotes the set of all nodes in the mesh and $J = \{j \in I : \omega_j \cap \mathcal{S} \neq \emptyset\}$ the set of nodes that form a partition of unity for g (Melenk and Babuška, 1996).

As shown by Ji (2001), g must meet specific conditions to ensure optimal rates of convergence in the energy norm and the local quantities of interest at the interface, such as the jump $\llbracket m_\gamma \text{Grad} u \rrbracket$ appearing in (2.4)₂. Here, we use the characteristic function for phase- β , in which case

$$g(\mathbf{x}, t) = \chi_\beta(\mathbf{x}, t) = \begin{cases} 0 & \mathbf{x} \in \mathcal{R}_\alpha(t), \\ 1 & \mathbf{x} \in \mathcal{R}_\beta(t). \end{cases} \quad (3.15)$$

As the discontinuity of χ_β coincides with the phase interface, the choice $g = \chi_\beta$ provides a mechanism for the approximation (3.14) to represent the geometry of the interface independent of the element boundaries.³ Furthermore, as the interface evolves, we update the enrichment function and the set J ; no remeshing is performed.

With the preceding definitions, we introduce a set

$$\{\Phi_r\}_{r=1}^N = \{\phi_i\}_{i=1}^{N_I} \cup \{\phi_j \chi_\beta\}_{j=1}^{N_J}, \quad (3.16)$$

of linearly independent functions Φ_r ; this set forms a basis for \mathcal{A}_m^h , where N_I and N_J denote, respectively, the number of elements in the sets I and J and $N = N_I + N_J$. We then represent \mathcal{A}_m^h as

$$\mathcal{A}_m^h = \text{span}\{\Phi_r\}_{r=1}^N. \quad (3.17)$$

We employ a Bubnov-Galerkin approximation and use this same set of functions to construct \mathcal{V}_m^h .⁴

The Lagrange multipliers are approximated by polynomial functions defined on the element interiors. Specifically,

$$\mathcal{L}_p^h = \text{span}\{\lambda_i\}_{i=1}^{N_I}, \quad \text{with} \quad \{\lambda_i \in P^k(\mathcal{S}_e)\},$$

where \mathcal{S}_e denotes the intersection of the interface with the element domain \mathcal{Q}_e . So, the approximation for the Lagrange multipliers is written as a linear combination

$$\mathbf{p}^h(\mathbf{x}, t) = \sum_i \mathbf{p}_i(t) \lambda_i(\mathbf{x}) \quad (3.18)$$

³Similar approaches have been employed by Krongauz and Belytschko (1998) and Sukumar et al. (2001). However, these approaches use continuous enrichment functions.

⁴The construction of \mathcal{V}_m^h only employs those functions Φ_k which vanish on the Dirichlet boundary $(\partial\mathcal{R})_m$.

of these functions. Details of the construction can be found in Dolbow et al. (2001) and Ji et al. (2002). A similar approximation is employed for the variations \mathbf{q}^h .

Substitution of the above and (3.14) into (3.12) results in a nonlinear system of equations in $\{\mathbf{c}_i, \mathbf{e}_j, \mathbf{p}_i\}$. We employ the standard Newton–Raphson procedure and solve the above with a sequence of linearized problems. These take the form

$$\mathbf{K}_f^{(n)} \Delta \mathbf{d}_f = \mathbf{r}^{(n)}, \quad (3.19)$$

with \mathbf{K}_f^n the tangent stiffness matrix at iteration n , \mathbf{r}^n the residual vector, and $\Delta \mathbf{d}_f$ the vector gathering the incremental degrees of freedom $\Delta \mathbf{c}_i$, $\Delta \mathbf{e}_j$, and $\Delta \mathbf{p}_i$. After solving the above, the solution is updated by $\mathbf{c}_i^{n+1} = \mathbf{c}_i^n + \Delta \mathbf{c}_i$, $\mathbf{e}_j^{n+1} = \mathbf{e}_j^n + \Delta \mathbf{e}_j$. The construction of the tangent stiffness matrix and residual vector requires the accurate integration of terms containing the classical and enriched basis functions over the element subdomains. The standard element-based quadrature routines are modified for those elements wherein the functions are discontinuous. Details for these modifications are provided by Dolbow et al. (2000).

3.2.2 Approximation for the diffusion potential u

The Galerkin approximation to variational boundary-value problem stated in Section 3.1.2 reads: find u^h in \mathcal{A}_p^h and k^h in \mathcal{L}_p^h such that

$$\left. \begin{aligned} \int_{\mathcal{R}} m_\gamma \text{Grad } u^h \cdot \text{Grad } w^h \, dv &= \int_{(\partial \mathcal{R})_f} h w^h \, da - \int_{\mathcal{S}} \llbracket k^h w^h \rrbracket \, da, \\ \int_{\mathcal{S}} \llbracket (u - u^h) l^h \rrbracket \, da &= 0, \end{aligned} \right\} \quad (3.20)$$

for all variations w^h of u^h and l^h and k^h belonging to \mathcal{V}_p^h and \mathcal{L}_p^h .

The approximation for the diffusion potential takes a form,

$$u^h(\mathbf{x}, t) = \sum_{i \in I} a_i(t) \phi_i(\boldsymbol{\xi}(\mathbf{x})) + \sum_{j \in J} b_j(t) \phi_j(\boldsymbol{\xi}(\mathbf{x})) \chi_\beta(\mathbf{x}, t), \quad (3.21)$$

in which $\{\phi_i\}$ is the set of nodal shape functions used in the approximation for the deformation. The above may be viewed as the scalar analog to (3.14). Here, the enrichment allows the approximation u^h to represent the arbitrary gradient discontinuities in the diffusion potential across the interface. The approximation for the Lagrange multiplier k takes a scalar form analogous to (3.18), viz.,

$$\overset{\pm}{k}^h(\mathbf{x}, t) = \sum_i \overset{\pm}{k}_i(t) \lambda_i(\mathbf{x}). \quad (3.22)$$

We again adopt a Bubnov–Galerkin approximation and write approximations for the variations w^h and l^h in the forms similar to (3.21) and (3.22), respectively. Upon substituting the approximations into the discrete weak form (3.20) and invoking the arbitrariness of the variations, we obtain a linear system of equations

$$\mathbf{K}_u \mathbf{d}_u = \mathbf{f}_u, \quad (3.23)$$

where \mathbf{d}_u gathers the degrees of freedom a_i , b_j , and k_i .

In closing this subsection we remark that the incorporation of intra-element discontinuities in the X-FEM approximation for both the diffusion potential (3.21) and the

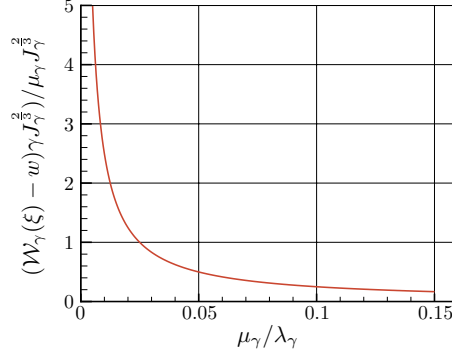
deformation (3.14) is distinct from other “embedded-discontinuity” approaches. We refer in particular to those techniques that employ incompatible modes to represent the discontinuity, such as the enhanced assumed strain approximations described in Armero and Garikipati (1996) and employed in silicon oxidation simulations by Rao et al. (2000) and Garikipati and Rao (2001). Such approximations represent viable alternatives to those presented here for representing the interface independently of the mesh. The advantage of the incompatible modes approach may rest in the availability of static condensation procedures, so that the size of the global system of equations remains fixed as the interface propagates. By the same token, the most effective incarnation of the incompatible modes approach results in somewhat undesirable asymmetric tangent stiffness matrices (Jirasek, 2000). By way of contrast, the Bubnov-Galerkin approximation adopted here leads to symmetric tangent stiffness matrices. The approximations presented in this subsection are therefore seen to be attractive alternatives for enriching classical finite element bases toward the goal of simulating evolving discontinuities without remeshing.

3.2.3 Staggered solution strategy

Equation (3.10) is solved using a uniform finite-difference stencil that is independent of the finite-element mesh (which may be unstructured). The technique employs standard upwinding algorithms taken from those developed for the solution of hyperbolic conservation laws (Osher and Sethian, 1988). The details of the coupling of fields between the finite difference grid and finite element mesh are given in Ji et al. (2002). The use of a structured finite difference stencil is advantageous from the perspective of conferring programming ease and ready access to the higher-order front representations described in Chopp (2001). We also note that in contrast to finite-element approximations for the nonlinear advection equation (Brooks and Hughes, 1982; Hughes, 1995), the present approach does not require the introduction of additional terms to stabilize the approximation.

We now describe the staggered solution strategy for the full system. Assuming that all fields and the geometry of the interface \mathcal{S} are known at some time t^n , the first step is to advect the level-set function through the system (3.10) and, thereby, to obtain the position of the interface at t^{n+1} . The nonlinear system (3.19) is then solved and the fields are post-processed to obtain the interfacial diffusion potential through the normal configurational force balance (2.4). Finally, the approximation for the diffusion potential is obtained by solving (3.23), completing the determination of all bulk fields at time t^{n+1} . The solution of (3.23) also yields the approximation for the Lagrange multipliers. These are used at time step t^{n+1} to evaluate the velocity of the interface through (3.9). The above process is then repeated. This strategy is exact and does not require iteration within a time step.

The success of the above solution strategy rests on the particular form of the evolution equations described in Section 2. Alternative formulations resulting in a more strongly coupled system might require modification to the above. For example, we remark that the choice of chemical potential as the primary variable describing mass transport leads to a number of advantages over other choices (such as the solute concentration). Firstly, we need not rely on numerical strategies to prevent artificially negative concentrations near the interface, such as the penalty formulation adopted by Garikipati and Rao (2001). Secondly, our bulk equations for solute balance and force balance do not involve rate terms. As a result, the stability of the scheme only appears to be governed by the standard CFL condition associated with the explicit update of the interface through the level set method. Although we have yet to rigorously prove this, we have not observed the sort of instabilities that can arise in staggered solution algorithms for coupled field phenomena (Zienkiewicz et al, 1988; Armero and Simo, 1992).

Figure 2: Relative importance of μ_γ and λ_γ to bulk strain-energy density.

4 Application: Swelling of a spherical specimen

4.1 Constitutive specialization

To model the deformational response of the bulk phases, we now specify a bulk strain-energy density W_γ for each phase γ . For simplicity, we assume that

$$W_\gamma(\mathbf{F}) = \frac{\mu_\gamma}{2} (|\mathbf{F}|^2 - 2J_\gamma^{\frac{2}{3}} \log \det(J_\gamma^{-\frac{1}{3}} \mathbf{F}) - 3J_\gamma^{\frac{2}{3}}) + \frac{\lambda_\gamma J_\gamma^{\frac{2}{3}}}{4} ((\det(J_\gamma^{-\frac{1}{3}} \mathbf{F}) - 1)^2 + \log^2 \det(J_\gamma^{-\frac{1}{3}} \mathbf{F})) + J_\gamma^{\frac{2}{3}} w_\gamma, \quad (4.1)$$

with $\mu_\gamma > 0$ and $\lambda_\gamma > 0$ mechanical moduli for phase γ and w_γ constant.

To illustrate some features of this choice, we consider pure dilatations $\mathbf{F} = \xi J_\gamma^{1/3} \mathbf{I}$, with $\xi > 0$, and introduce

$$\mathcal{W}_\gamma(\xi) = W_\gamma(\xi J_\gamma^{\frac{1}{3}} \mathbf{I}). \quad (4.2)$$

Then, for all admissible ξ , direct calculations show that, by the assumed positivity of μ_γ and λ_γ ,

$$\mathcal{W}_\gamma(\xi) \geq w_\gamma J_\gamma^{\frac{2}{3}} \quad \text{and} \quad \frac{d^2 \mathcal{W}_\gamma(\xi)}{d\xi^2} \geq 0. \quad (4.3)$$

Hence, when restricted to pure dilatations, W_γ is bounded below by $J_\gamma^{2/3} w_\gamma$ and is convex. Further, since $\min_{\xi > 0} \mathcal{W}_\gamma(\xi) = \mathcal{W}_\gamma(1) = w_\gamma J_\gamma^{2/3}$, J_γ is the energetically-preferred dilatation for phase γ .

A sense of the relative importance of the moduli μ_γ and λ_γ is given by considering the scaled difference $(\mathcal{W}_\gamma(\xi) - w_\gamma J_\gamma^{2/3}) / \mu_\gamma J_\gamma^{2/3}$ for a range of the dimensionless parameter $\mu_\gamma / \lambda_\gamma$ (Figure 2).

Since a strain-energy density can be determined only up to an arbitrary additive constant, it is the difference $\llbracket J_\gamma^{1/3} w_\gamma \rrbracket = J_\beta^{1/3} w_\beta - J_\alpha^{1/3} w_\alpha$ rather than the individual values $J_\gamma^{1/3} w_\gamma$ that are important in what follows.

Next, an easy calculation shows that

$$\frac{\partial W_\gamma(\mathbf{F})}{\partial \mathbf{F}} = \mu_\gamma (\mathbf{F} - J_\gamma^{\frac{2}{3}} \mathbf{F}^{-\top}) + \frac{\lambda_\gamma J_\gamma^{\frac{2}{3}}}{2} \left((\det(J_\gamma^{-\frac{1}{3}} \mathbf{F}) - 1) \det(J_\gamma^{-\frac{1}{3}} \mathbf{F}) + \log \det(J_\gamma^{-\frac{1}{3}} \mathbf{F}) \right) \mathbf{F}^{-\top}. \quad (4.4)$$

Thus,

$$\left. \frac{\partial W_\gamma(\mathbf{F})}{\partial \mathbf{F}} \right|_{\mathbf{F}=J_\gamma^{\frac{1}{3}}\mathbf{I}} = \mathbf{0}, \quad (4.5)$$

and we conclude that phase γ is stress-free at the energetically-preferred dilatation $\mathbf{F} = J_\gamma^{1/3}\mathbf{I}$. Further, a lengthy calculation yields

$$\begin{aligned} \frac{\partial^2 W_\gamma(\mathbf{F})}{\partial \mathbf{F}^2} &= \mu_\gamma(\mathbf{I} \otimes \mathbf{I} + J_\gamma^{\frac{2}{3}} \mathbb{T}(\mathbf{F}^{-\top} \boxtimes \mathbf{F}^{-\top})) \\ &\quad - \frac{\lambda_\gamma J_\gamma^{\frac{2}{3}}}{2} ((\det(J_\gamma^{-\frac{1}{3}} \mathbf{F}) - 1) \det(J_\gamma^{-\frac{1}{3}} \mathbf{F}) + \log \det(J_\gamma^{-\frac{1}{3}} \mathbf{F})) \mathbb{T}(\mathbf{F}^{-\top} \boxtimes \mathbf{F}^{-\top}) \\ &\quad + \frac{\lambda_\gamma J_\gamma^{\frac{2}{3}}}{2} ((2 \det(J_\gamma^{-\frac{1}{3}} \mathbf{F}) - 1) \det(J_\gamma^{-\frac{1}{3}} \mathbf{F}) + 1) \mathbf{F}^{-\top} \otimes \mathbf{F}^{-\top}, \end{aligned} \quad (4.6)$$

where $\mathbf{H} \boxtimes \mathbf{K}$, \mathbb{T} , $\mathbf{H} \otimes \mathbf{K}$ are the fourth-order tensors defined (Del Piero, 1979) so that, for any second-order tensor \mathbf{A} , $(\mathbf{H} \boxtimes \mathbf{K})\mathbf{A} = \mathbf{H}\mathbf{A}\mathbf{K}^\top$, $\mathbb{T}\mathbf{A} = \mathbf{A}^\top$, and $(\mathbf{H} \otimes \mathbf{K})\mathbf{A} = (\mathbf{K} \cdot \mathbf{A})\mathbf{H}$. An immediate consequence of (4.6) is that

$$\left. \frac{\partial^2 W_\gamma(\mathbf{F})}{\partial \mathbf{F}^2} \right|_{\mathbf{F}=J_\gamma^{\frac{1}{3}}\mathbf{I}} = \mu_\gamma(\mathbf{I} \otimes \mathbf{I} + \mathbb{T}(\mathbf{I} \boxtimes \mathbf{I})) + \lambda_\gamma \mathbf{I} \otimes \mathbf{I}. \quad (4.7)$$

Thus, μ_γ and λ_γ correspond to conventional shear and Lamé moduli for infinitesimal deviations from the stress-free state in phase γ . A more far-reaching consequence of (4.6) is that, by the assumed positivity of μ_γ and λ_γ ,

$$\begin{aligned} \mathbf{a} \otimes \mathbf{b} \cdot \left(\frac{\partial^2 W_\gamma(\mathbf{F})}{\partial \mathbf{F}^2} \mathbf{a} \otimes \mathbf{b} \right) &= \mu_\gamma (|\mathbf{a}|^2 |\mathbf{b}|^2 + 2J_\gamma^{\frac{2}{3}} (\mathbf{F}^{-1} \mathbf{a} \cdot \mathbf{b})^2) \\ &\quad + \frac{\lambda_\gamma J_\gamma^{\frac{2}{3}}}{2} \left(1 + \left(\frac{\det \mathbf{F}}{J_\gamma} \right)^2 - \frac{1}{2} \log \left(\frac{\det \mathbf{F}}{J_\gamma} \right) \right) (\mathbf{F}^{-1} \mathbf{a} \cdot \mathbf{b})^2 > 0. \end{aligned} \quad (4.8)$$

Thus, the strain-energy density of each phase is rank-one convex.

Without loss of generality, we assume that $J_\beta = 1$. Then, since α is the swelled phase, we must necessarily have $J_\alpha > 1$. The presence of such a “swelling parameter” in the model accounts phenomenologically for the microphysical mechanisms associated with the conformational changes that occur during transitions between the swelled and collapsed phases. A more accurate model would account explicitly for the coupling between network distortion and chemistry that underlies such mechanisms. Nevertheless, while the model used here does not provide a direct link to molecular-scale details such as cross-link density and chain conformation, it can be easily correlated with micro-scale experimental measurements. A similar approach has been successfully developed by Barriere and Leibler (2003); the distinction of the present model is the emphasis on the two distinct phases.

4.2 Kinematical specialization

We consider the problem of a traction-free specimen suspended in a solvent-rich reservoir of solution with uniform diffusion potential. We assume that, in the reference configuration, the specimen occupies the spherical region $\mathcal{R} = \{\mathbf{x} : |\mathbf{x}| \leq R\}$. Writing

$$\mathbf{e} = \frac{\mathbf{x}}{|\mathbf{x}|}, \quad (4.9)$$

the requirement that the specimen be traction-free yields

$$\mathbf{S}\mathbf{e}|_{\partial \mathcal{R}} = \mathbf{0}. \quad (4.10)$$

Further, writing $U(t)$ for the value of the diffusion potential of the reservoir at time t , we have

$$u|_{\partial\mathcal{R}} = U. \quad (4.11)$$

We restrict attention to circumstances in which the deformation and the diffusion potential depend at most on radial position $r = |\mathbf{x}|$ and time t , viz.,

$$\mathbf{y}(\mathbf{x}, t) = y(r, t)\mathbf{e} \quad \text{and} \quad u(\mathbf{x}, t) = u(r, t). \quad (4.12)$$

Consistent with these assumptions, we suppose that the interface is concentric, and write $\mathcal{S}(t) = \{\mathbf{x} : |\mathbf{x}| = s(t)\}$ for its position at time t . Anticipating that swelling should proceed from the boundary inwards towards the center of the specimen,

$$\mathbf{n} = -\mathbf{e}, \quad \mathbf{K} = \text{Grad}_s \mathbf{n} = -\frac{2}{s}, \quad \text{and} \quad \mathbf{v} = -\dot{s}. \quad (4.13)$$

We use g' to denote the partial derivative of a field g with respect to r . Thus, by (4.12)₁, the deformation gradient has the particular form

$$\mathbf{F}(r, t) = y'(r, t)\mathbf{e} \otimes \mathbf{e} + \frac{y(r, t)}{r}(\mathbf{I} - \mathbf{e} \otimes \mathbf{e}) \quad (4.14)$$

and the associated Jacobian is given by

$$J(r, t) = \det \mathbf{F}(r, t) = \frac{y^2(r, t)y'(r, t)}{r^2} > 0. \quad (4.15)$$

Since $\det \mathbf{F} > 0$, it follows that y must obey $y(r, t) \geq 0$ and $y'(r, t) > 0$ for $0 < r \leq R$, as well as

$$y(r, t) \sim r \quad \text{and} \quad y'(r, t) \sim 1 \quad \text{as} \quad r \rightarrow 0. \quad (4.16)$$

4.3 Reduced governing equations

4.3.1 Bulk equations

In view of (4.4), (4.14), and (4.15),

$$\frac{\partial W_\gamma(\mathbf{F})}{\partial \mathbf{F}} = S_\parallel \mathbf{e} \otimes \mathbf{e} + S_\perp (\mathbf{I} - \mathbf{e} \otimes \mathbf{e}), \quad (4.17)$$

with

$$S_\parallel(r, t) = \mu_\gamma \left(y'(r, t) - \frac{J_\gamma^{\frac{2}{3}}}{y'(r, t)} \right) + \frac{\lambda_\gamma J_\gamma^{\frac{2}{3}} D(r, t)}{2y'(r, t)} \quad (4.18)$$

and

$$S_\perp(r, t) = \mu_\gamma \left(\frac{y(r, t)}{r} - \frac{J_\gamma^{\frac{2}{3}} r}{y(r, t)} \right) + \frac{\lambda_\gamma J_\gamma^{\frac{2}{3}} r D(r, t)}{2y(r, t)} \quad (4.19)$$

the components of radial and hoop stress, and (cf. (4.15))

$$D(r, t) = \frac{J(r, t)}{J_\gamma} \left(\frac{J(r, t)}{J_\gamma} - 1 \right) + \log \left(\frac{J(r, t)}{J_\gamma} \right). \quad (4.20)$$

Thus, the deformational force balance (2.3)₁ reduces to the scalar equation $(r^2 S_\parallel(r, t))' = 2r S_\perp(r, t)$, which, by (4.18) and (4.19), can be written as

$$\begin{aligned} & \left(\mu_\gamma r^2 \left(y'(r, t) - \frac{J_\gamma^{\frac{2}{3}}}{y'(r, t)} \right) + \frac{\lambda_\gamma J_\gamma^{\frac{2}{3}} r^2 D(r, t)}{2y'(r, t)} \right)' \\ & = 2\mu_\gamma \left(y(r, t) - \frac{J_\gamma^{\frac{2}{3}} r^2}{y(r, t)} \right) + \frac{\lambda_\gamma J_\gamma^{\frac{2}{3}} r^2 D(r, t)}{y(r, t)}. \end{aligned} \quad (4.21)$$

Similarly, by (4.12)₂, the solute balance (2.3)₂ simplifies to

$$m_\gamma(r^2 u'(r, t))' = 0. \quad (4.22)$$

4.3.2 Interfacial equations

On appealing to (4.17) and (4.13)₁, the deformational force balance (2.4)₁ reduces to the scalar equation $\llbracket S_{\parallel} \rrbracket = 0$, which, by (4.18), can be written as

$$\left[\mu_\gamma \left(y'(\mathbf{s}(t), t) - \frac{J_\gamma^{\frac{2}{3}}}{y'(\mathbf{s}(t), t)} \right) + \frac{\lambda_\gamma J_\gamma^{\frac{2}{3}} D(\mathbf{s}(t), t)}{2y'(\mathbf{s}(t), t)} \right] = 0. \quad (4.23)$$

Similarly, by (4.12)₂ and (4.13)_{1,3}, the solute balance (2.4)₂ simplifies to

$$\dot{\mathbf{s}}(t) = - \frac{\llbracket m_\gamma u'(\mathbf{s}(t), t) \rrbracket}{\llbracket c_\gamma \rrbracket}. \quad (4.24)$$

Finally, by (4.1), (4.14), (4.17), (4.18), (4.19), and (4.13), the normal configurational force balance (2.4) becomes

$$\begin{aligned} \llbracket c_\gamma \rrbracket u(t) = & - \frac{2\sigma}{\mathbf{s}(t)} - \frac{1}{2} \left[\mu_\gamma \left((y'(\mathbf{s}(t), t))^2 + \frac{2y^2(\mathbf{s}(t), t)}{\mathbf{s}^2(t)} + 2J_\gamma^{\frac{2}{3}} \log \left(\frac{J(\mathbf{s}(t), t)}{J_\gamma} \right) - 3J_\gamma^{\frac{2}{3}} \right) \right] \\ & + \frac{1}{4} \left[\lambda_\gamma J_\gamma^{\frac{2}{3}} \left(\left(\frac{J(\mathbf{s}(t), t)}{J_\gamma} - 1 \right)^2 + \log^2 \left(\frac{J(\mathbf{s}(t), t)}{J_\gamma} \right) - 6D(\mathbf{s}(t), t) \right) \right] + \llbracket J_\gamma^{\frac{2}{3}} w_\gamma \rrbracket. \end{aligned} \quad (4.25)$$

In view of (4.12), the conditions (2.1) and (2.2) of coherency and local equilibrium hold if and only if

$$\llbracket y(\mathbf{s}(t), t) \rrbracket = 0 \quad \text{and} \quad \llbracket u(\mathbf{s}(t), t) \rrbracket = 0. \quad (4.26)$$

4.3.3 Boundary conditions

The asymptotic restriction (4.16) yields the condition

$$y(0, t) = 0 \quad (4.27)$$

at the center of the specimen. By (4.17), the traction-free condition (4.10) reduces to

$$\mu_\alpha \left(y'(R, t) - \frac{J_\alpha^{\frac{2}{3}}}{y'(R, t)} \right) + \frac{\lambda_\alpha J_\alpha^{\frac{2}{3}} J(R, t)}{2y'(R, t)} = 0. \quad (4.28)$$

The requirement that u be radially-symmetric requires that

$$u'(0, t) = 0. \quad (4.29)$$

By (4.12)₂, (4.11) becomes

$$u(R, t) = U(t). \quad (4.30)$$

4.3.4 Initial condition

We suppose that the position of the interface is given initially, so that

$$\mathbf{s}(0) = \mathbf{s}_0, \quad \text{with } 0 \leq \mathbf{s}_0 \leq R. \quad (4.31)$$

4.4 Analytical observations

Equations (4.21)–(4.31) form an initial-boundary-value problem for determining the bulk deformation y , the bulk diffusion potential u , the interfacial position \mathbf{s} , and the interfacial diffusion potential \mathbf{u} (with the understanding that $u(\mathbf{s}(t), t) = \mathbf{u}(t)$ for each time t).

If \mathbf{s} is treated as given, the bulk and interfacial deformational force balances (4.21) and (4.23), the condition (4.26)₁ of coherency, and the boundary conditions (4.27) and (4.28) form a problem that might, in principle, be solved to determine y parametrically in terms of \mathbf{s} and the parameters μ_γ , λ_γ , and J_γ . Particular (time-independent) solutions which can be easily verified are

$$y(r) = J_\alpha^{\frac{1}{3}} r, \quad (4.32)$$

corresponding to a specimen which is completely swelled ($\mathbf{s} = 0$), and

$$y(r) = J_\beta^{\frac{1}{3}} r, \quad (4.33)$$

corresponding to a specimen which is fully collapsed ($\mathbf{s} = R$). However, for $0 < \mathbf{s} < R$, we have not been able to determine y in closed form.

Nevertheless, the bulk solute balance (4.22), the condition (4.26)₂ of local chemical equilibrium, and the boundary conditions (4.29) and (4.30) can be solved easily to obtain an expression

$$u(r, t) = \begin{cases} \mathbf{u}(t), & 0 < r \leq \mathbf{s}(t), \\ U(t) - \frac{\mathbf{s}(t)(U(t) - \mathbf{u}(t))}{R - \mathbf{s}(t)} \left(\frac{R}{r} - 1 \right), & \mathbf{s}(t) \leq r < R, \end{cases} \quad (4.34)$$

for u in terms of \mathbf{s} , \mathbf{u} , and the diffusion potential U in the reservoir. This expression shows that, at each time t , the diffusion potential of the collapsed phase is uniform and equal to the interfacial diffusion potential $\mathbf{u}(t)$. Further, unless $U(t) = \mathbf{u}(t)$, (4.34) shows that the diffusion potential of the swelled phase varies monotonically with r —decreasing or increasing from the boundary value $U(t)$ to the interfacial value $\mathbf{u}(t)$ when $\mathbf{u}(t) < U(t)$ and $\mathbf{u}(t) > U(t)$, respectively.

Not covered by (4.34) are the (time-independent) states of complete swelling ($\mathbf{s} = 0$) and collapse ($\mathbf{s} = R$) corresponding to fields y of the forms (4.32) and (4.33), respectively. In both of these cases, (4.34) is replaced by the (time-independent) expression

$$u(r) = U. \quad (4.35)$$

It follows that completely swelled and collapsed states can only occur if the diffusion potential of the specimen is uniform and equal to that of the reservoir.

As a simple consequence of (4.34), we may rewrite the interfacial solute balance (4.24) in the form

$$\dot{\mathbf{s}}(t) = - \frac{m_\alpha}{\llbracket c_\gamma \rrbracket} \frac{R(U(t) - \mathbf{u}(t))}{\mathbf{s}(t)(R - \mathbf{s}(t))}. \quad (4.36)$$

Together with the initial condition (4.31), (4.36) yields an initial-value problem for \mathbf{s} .⁵ At any time t , the instantaneous kinetic response of the gel can be characterized by the velocity $\dot{\mathbf{s}}$ of the interface. Bearing in mind that $c_\alpha > c_\beta$, $m_\gamma > 0$, and (4.36),

$$\dot{\mathbf{s}}(t) \begin{cases} < 0 & \text{if } U(t) > \mathbf{u}(t), \\ = 0 & \text{if } U(t) = \mathbf{u}(t), \\ > 0 & \text{if } U(t) < \mathbf{u}(t). \end{cases} \quad (4.37)$$

⁵Using the normal configurational force balance (4.25) in (4.36) leads to an alternative version of the interfacial solute balance which, granted knowledge of y constitutes a nonlinear differential equation for \mathbf{s} . For brevity, we do not reproduce this equation here.

Hence, whether the specimen swells or shrinks at an instant t is dictated entirely by the difference between the diffusion potential $U(t)$ of the reservoir and the diffusion potential $u(t)$ in the collapsed phase. When $u(t) < U(t)$, the interface moves toward the center of the specimen, which increases in volume as the swelled phase grows at the expense of the collapsed phase. When $u(t) = U(t)$, the diffusion potential is uniform and the volumes occupied by the phases are fixed. When $u(t) > U(t)$, the interface moves toward the boundary of the specimen, which decreases in volume as the collapsed phase grows at the expense of the swelled phase.

Returning to (4.36), we note that, provided the time-dependence of the difference $U - u$ is weak in the sense that

$$U(t) - u(t) \approx U_0, \quad (4.38)$$

with U_0 constant, then, bearing in mind the initial condition (4.31), the differential equation (4.36) can be integrated in closed form to yield \mathbf{s} . In the special case where the specimen is initially collapsed, this expression predicts that the time required for complete swelling of the specimen is finite and given by

$$\tau = \frac{[[c_\gamma]]R^2}{6m_\alpha U_0}. \quad (4.39)$$

Despite the unrealistic nature of the assumption (4.38), the prediction (4.39) of swelling time concurs with experimental observations, which indicate that the time required for complete swelling of a collapsed specimen scales with the square of the initial radius of the specimen (Tanaka et al, 1985; Matsuo and Tanaka, 1989)

4.5 Numerical results

In view of (4.34) and (4.36), the initial-boundary-value problem (4.21)–(4.31) is equivalent to a reduced problem for y , u , and \mathbf{s} and consisting of (4.21), (4.23), (4.25), (4.26)₁, (4.27), (4.28), and (4.31). This reduction occurs solely due to the radial symmetry of the problem at hand. Under more general circumstances, (4.34) would be replaced by an integral representation for the diffusion potential and the corresponding reduced problem would be nonlocal. With a view to studying problems involving specimens of arbitrary geometry, we use the numerical method described in Section 3.2 to study the initial-boundary-value problem (4.21)–(4.31).

In the sections that follow, we conduct studies that examine how particular material parameters in the model influence the numerical predictions. The baseline quantities for these studies, considering a gel with an initial radius of $R = 1.00$ cm, a characteristic swelling time of $T = 100$ s, and a characteristic diffusion potential of $\Theta = 1.00$ J, are provided in Table 1. We begin by investigating static solutions that result on fixing the position of the interface along with the diffusion potential of the reservoir. We then study problems in which the interface is allowed to evolve and equilibrate under the influence of a given diffusion potential of the reservoir. Finally, we consider the response of the specimen to cyclic changes of the diffusion potential of the reservoir.

4.5.1 Static two-phase states

Assuming that the value U of the diffusion potential of the reservoir is time-independent, we consider the artificial problem of constructing solutions for given fixed positions \mathbf{s} of the interface. In this case, the problem reduces to determining t -independent y and u from (4.21)–(4.30), excepting (4.24).

Property	Normalization	Collapsed phase (β)	Swelled phase (α)
c_γ	c_γ	0.2	0.1
m_γ	$\frac{m_\gamma T}{R^2(c_\beta - c_\alpha)\Theta}$	0.001	0.002
σ	$\frac{\sigma}{R(c_\beta - c_\alpha)}$	0.01	0.01
μ_γ	$\frac{\mu_\gamma}{(c_\beta - c_\alpha)\Theta}$	200.0	100.0
λ_γ	$\frac{\lambda_\gamma}{(c_\beta - c_\alpha)\Theta}$	10000	5000
J_γ	J_γ	1.0	10.0
w_γ	$\frac{w_\gamma}{(c_\beta - c_\alpha)\Theta}$	0.0	20.0

Table 1: Baseline material properties and parameters used in the parametric studies. Normalized quantities are provided based on a gel with radius $R = 1.00$ cm, characteristic swelling time $T = 100$ s, and characteristic diffusion potential $\Theta = 1.00$ J.

We first examine the influence of the preferred dilation $J_\alpha > 1$ of the swelled phase and the mechanical moduli μ_γ and λ_γ on the net volumetric expansion of the specimen. To quantify this change, we introduce the macroscopic swelling ratio

$$Q = \frac{y^3(R)}{R^3}. \quad (4.40)$$

An upper bound Q_{\max} for this ratio is provided by the completely-swelled state (4.32), which yields $Q_{\max} = J_\alpha$. We note that this bound is independent of the mechanical moduli μ_γ and λ_γ .

We now examine static two-phase states for a reservoir level of $U = 1.0$ J and incremental interface positions corresponding to $s/R = 1.0, 0.8, 0.6, 0.4, 0.2$, and 0.0 . The dimensionless deformation y/R and diffusion potential u/Θ are shown in Figures 3 and 4. The numerical approximation for the deformation exactly reproduces the solutions (4.32) and (4.33) when the interface is fixed at $s = 0$ and $s = R$, respectively. For $0 < s < R$, the numerical approximation for the diffusion potential is also seen to be indistinguishable from the analytically determined expression (4.34) for u . We note that when the interface is located on the interior of the specimen, its position is clearly delineated by discontinuities in both y' and u' .

Figures 5–6 depict, for the same incremental interface positions used in plotting Figures 3–4, the dimensionless radial stress $S_{\parallel}/(\mu_\beta - \mu_\alpha)$ and the dimensionless hoop stress $S_{\perp}/(\mu_\beta - \mu_\alpha)$ as functions of the dimensionless radial position r/R . These plots indicate that the collapsed phase is not stress-free. The mismatch in material moduli at the interface induces a compressive hoop stress in the swelled phase and a tensile hoop stress in the collapsed phase, as shown in Figure 6. To satisfy force balance in the bulk, this gives rise to a non-zero radial stress in the collapsed phase. Satisfaction of the bulk deformational balance then entails a non-trivial radial stress in the collapsed phase.

From Figure 5, we observe that the interfacial force balance and traction-free boundary condition are weakly enforced by the approximation. Finally, we remark that the

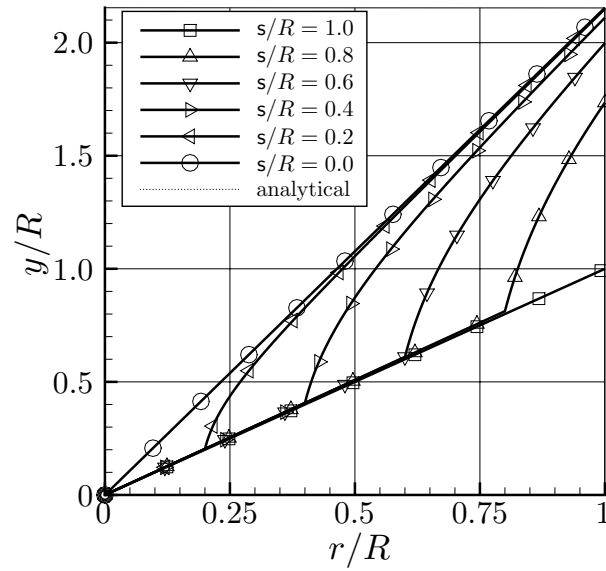


Figure 3: Normalized deformation for equally-spaced intervals of interfacial position along the gel radius.

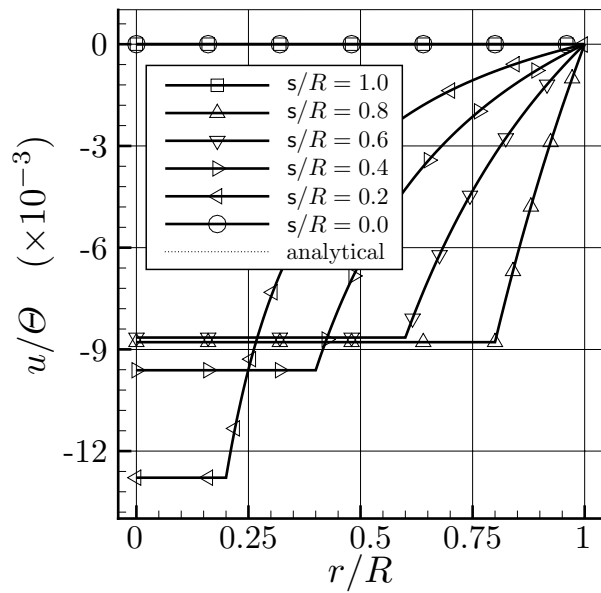


Figure 4: Normalized diffusion potential at incremental interface locations.

stress components are identical in the collapsed phase, i.e., $S_{\parallel} = S_{\perp}$ for $r < s$.

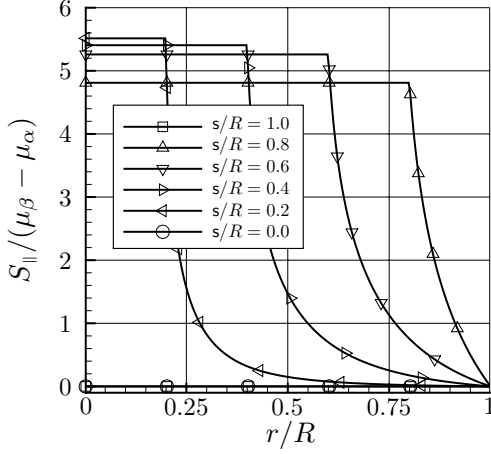


Figure 5: Normalized radial stress at incremental radial locations.

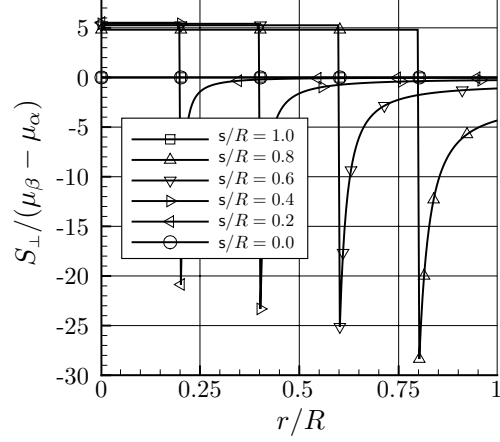


Figure 6: Normalized hoop stress at incremental interface locations.

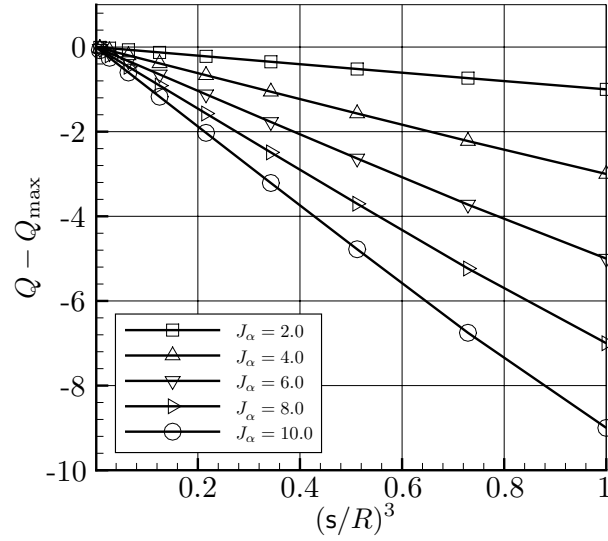
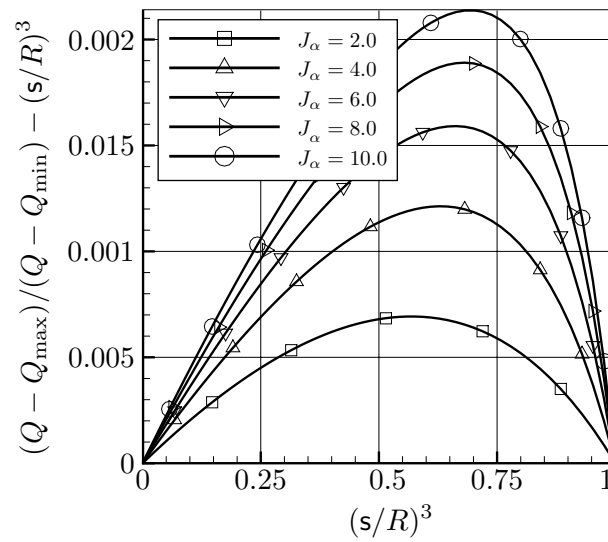
For static two-phase states, the deformation field y/R is a nonlinear function of both the parameters J_{γ} and w_{γ} as well as the moduli μ_{γ} and λ_{γ} . It is independent of the diffusion potential U of the reservoir. To convey the complex relationships as concisely as possible, we now examine how these properties influence the swelling ratio Q as a function of s/R . Figure 7 plots $Q - Q_{\max}$ against $(s/R)^3$ for various values of the parameter J_{α} . The curves appear to be linear, and a simple analysis yields

$$Q - Q_{\max} \approx (1 - J_{\alpha}) \left(\frac{s}{R}\right)^3.$$

Equivalently, since $Q_{\max} = J_{\alpha}$ and $Q_{\min} = 1$, we may rewrite this as

$$\frac{Q - Q_{\max}}{Q_{\min} - Q_{\max}} \approx \left(\frac{s}{R}\right)^3. \quad (4.41)$$

A plot of the deviation from this relationship is shown in Figure 8 for the same choices of J_{α} . Analogous studies indicate that the deviation is relatively insensitive to variations in λ_{γ} , μ_{γ} , and w_{γ} . The dilatation parameter J_{α} therefore appears to be the dominant factor in determining the swelling ratio Q .

Figure 7: Influence of J_α on swelling ratio.Figure 8: Deviation from scaling relationship (4.41) with various J_α .

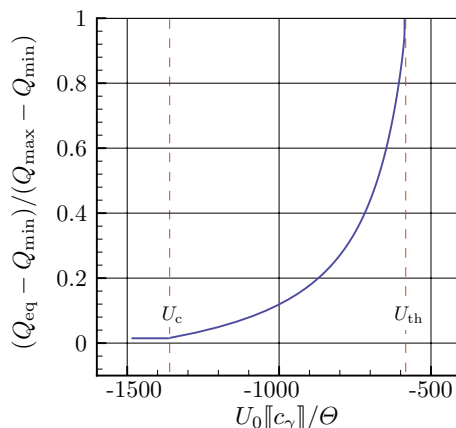


Figure 9: A “breakthrough” curve for the equilibrium swelling ratio Q_{eq} as a function of constant reservoir potential U_0 . This curve is generated numerically by solving (4.21)–(4.30), with $U = U_0$ for a sequence of U_0 and $\mathbf{s}_0 = R$. The calculations are performed for a sufficiently large interval of time such that the interface comes to an equilibrium position, yielding Q_{eq} .

4.5.2 Time-dependent response

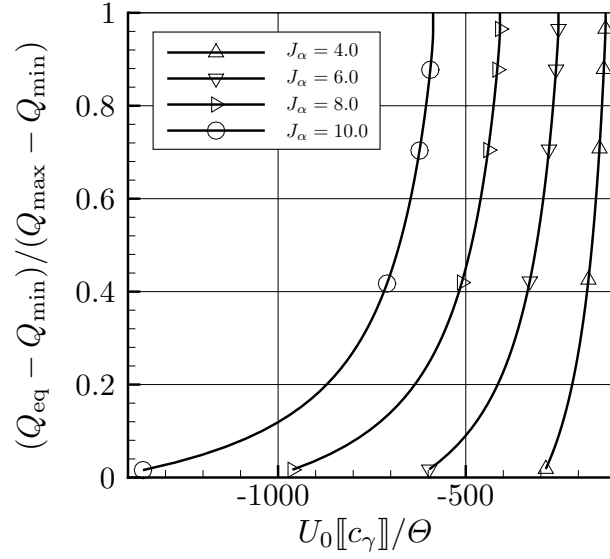
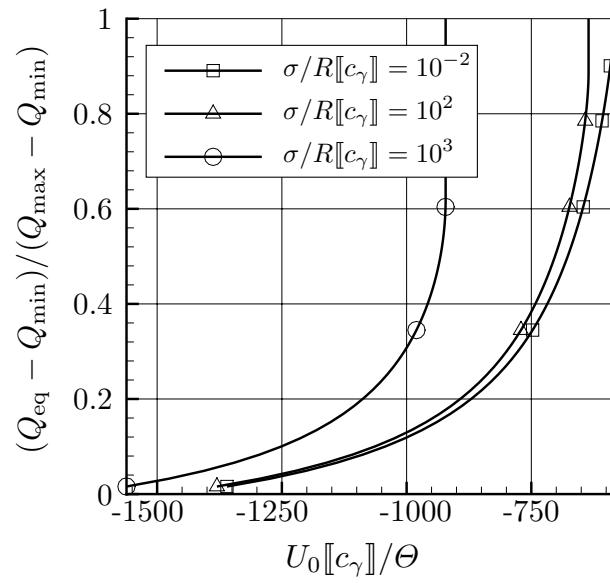
We now present solutions to the initial-boundary-value problem (4.21)–(4.31). We begin by considering the initial and boundary conditions

$$\mathbf{s}_0 = R, \quad U = U_0 = \text{constant}, \quad (4.42)$$

corresponding to a specimen that is initially collapsed, with the diffusion potential of the reservoir held constant.

As discussed in Section 4.4, the tendency for the specimen to shrink or swell depends on the difference $U - u$ of the diffusion potential U of the reservoir and that u on the interface. If at some time t_* these two quantities come into balance, i.e. $u(t_*) = U$, the position of the interface comes to a rest and the system reaches a state of equilibrium. Using the values of the material properties given in Table 1, we have obtained a series of solutions to the above over a range of U . Figure 9 plots the equilibrium swelling ratio Q_{eq} for this range of diffusion potential of the reservoir. We note that for U below a minimum level identified on the plot as U_c , the equilibrium state is identical to the initial condition specified above and the gel remains as a single collapsed phase. Above a threshold level identified as U_{th} , the equilibrium state corresponds to a gel that is fully swelled. Hereafter, we refer to such a plot as the $Q - U$ breakthrough curve.

Of the material parameters which enter our model, the $Q - U$ breakthrough curves are most sensitive to variations in J_γ , σ , and c_γ . As implied by the normalization used in Figure 9, the curves exhibit a simple scaling with the jump $[[c_\gamma]]$ of the polymer concentration between the swelled and collapsed phases. If $[[c_\gamma]]$ is doubled, for example, then both U_c and U_{th} decrease by half. The breakthrough curves for various J_α are shown in Figure 10. Clearly, increasing J_α lowers both the equilibrium diffusion potential U_c for the collapsed phase and threshold level U_{th} for the swelled phase. These curves were generated for the various J_α while holding the remaining material parameters fixed at the values listed in Table 1. Similar breakthrough curves for various choices of the interfacial energy density σ are shown in Figure 11. We note that a marked deviation from the curve shown in Figure 9 is only observed when the dimensionless quantity $\sigma/R[[c_\gamma]]$ becomes sufficiently large.

Figure 10: “Breakthrough” curves for various J_α .Figure 11: “Breakthrough” curves for various interfacial energy densities σ .

With the data from the above breakthrough curves, we next examine the influence of the material properties on the swelling kinetics by investigating solutions to (4.21)–(4.31) with the initial and boundary conditions

$$s_0 = R, \quad U(t) = U_c + \alpha H(t), \quad (4.43)$$

where H is the Heaviside function. These conditions correspond to a specimen that is initially in a collapsed equilibrium state and is subsequently subjected to a step change in the reservoir potential. To trigger an eventual transition to a completely swelled state, we set $\alpha = 1.05(U_{\text{th}} - U_c)$. Associated with this initial-boundary-value problem we introduce a characteristic swelling time τ for the gel, defined as the time at which $s(\tau) = 0$.

Figure 12 plots the dimensionless interface position as a function of dimensionless time for specimens with initial radii of 1.0 cm, 2.0 cm, 4.0 cm, and 8.0 cm. These curves were obtained using the parameter values given in Table 1 and the values of U_c and U_{th} . We note that these curves bear a strong qualitative resemblance to the experimental results of Gehrke et al. (1992). Since $T = 100$ s, these results indicate swelling times on the order of minutes for the centimeter-scale gels. Such swelling times are also consistent with the experimental measurements of Gehrke et al. (1992).

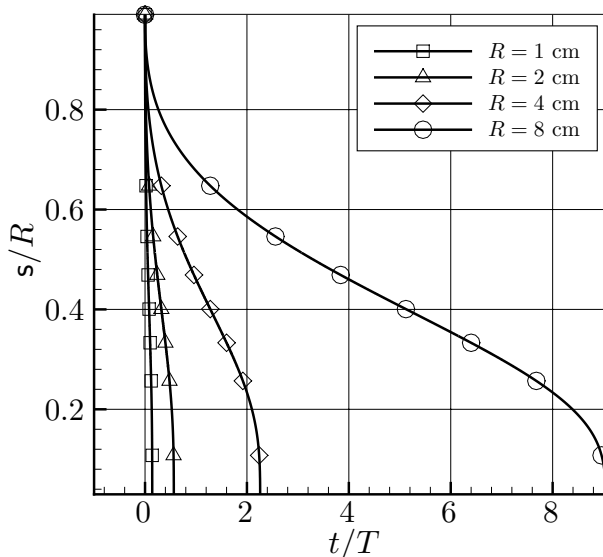


Figure 12: Normalized interface position with time for gels of increasing radii.

We repeat the above calculations for the same set of initial gel radii and for $J_\alpha = 4.0, 6.0, 8.0,$ and 10.0 . For each J_α , the values of U_c and U_{th} obtained from Figure 10 are employed in (4.43). The dimensionless characteristic swelling time is plotted against the square of the gel radius in Figure 13. The results clearly indicate that $\tau \sim R^2$, with increasing J_α corresponding to faster characteristic swelling times.

As discussed in Section 4.4, the scaling $\tau \sim R^2$ is expected if the difference $U - u$ is approximately constant. For comparison, Figure 14 shows the analytical prediction given by (4.39) plotted alongside the numerical results for the limiting choices of J_α . For the analytical prediction, the difference $U - u$ was approximated as $U - U_{\text{th}}$. The plots indicate that the analytical prediction yields swelling times that are approximately 50% longer than those obtained numerically.

The difference between the analytical and numerical predictions is attributable to the fact that $U - u$ is not constant in time. A plot of this quantity, normalized by Θ , is

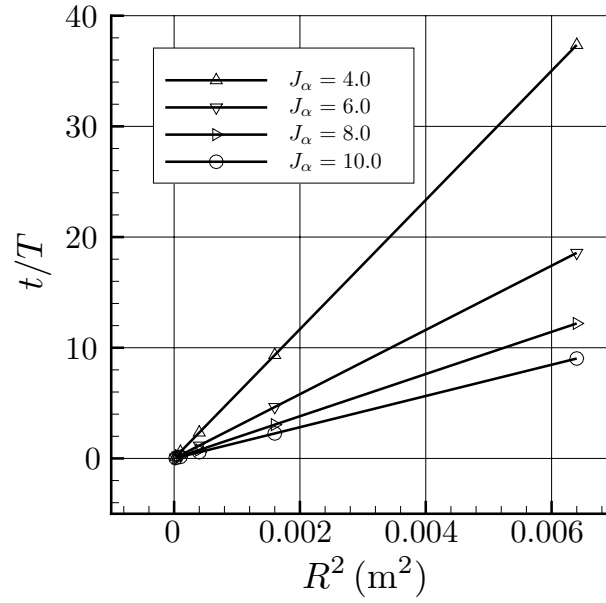


Figure 13: Characteristic swelling times as a function of initial gel radius squared for various J_α .

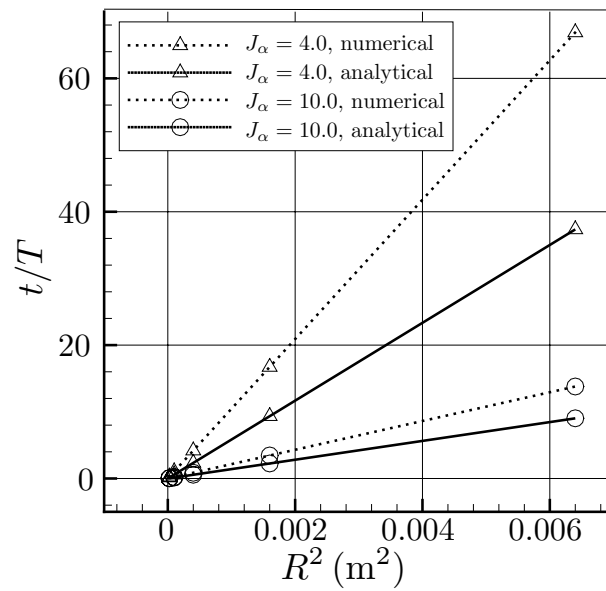


Figure 14: Comparison of numerical and analytical (4.39) characteristic swelling times.

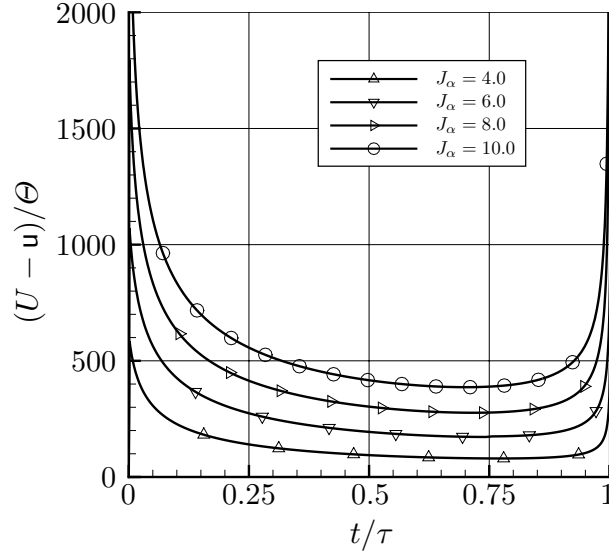


Figure 15: Diffusion potential difference as a function of time for various J_α .

shown for dimensionless time t/τ in Figure 15 for the same choices of J_α used to generate Figure 13. This plot indicates that deviations from the scaling $\tau \sim R^2$ are most likely to occur during the early and late stages of the swelling. In particular, $(U - u)/\Theta$ increases sharply as the characteristic swelling time τ is approached. In this regime, the interface is nearing the center of the specimen and the first term $-2\sigma/s$ on the right side of (4.25) is dominant.

The characteristic swelling time τ is also sensitive to the molecular mobility m_α in the swelled phase, $[[c_\gamma]]$, and σ . The influence of the mobility m_α on the characteristic swelling time follows directly from (4.36). Doubling the mobility in the swelled phase simply doubles the velocity of the interface, and therefore decreases the swelling time by a factor of two. Similarly, the interface velocity is inversely proportional to the jump $[[c_\gamma]]$ in polymer chain concentration. As discussed above, the levels U_c and U_{th} are also inversely proportional to $[[c_\gamma]]$. It follows that the characteristic swelling times obtained using (4.43) are proportional to $1/[[c_\gamma]]^2$.

The interfacial energy density σ does not influence the scaling $\tau \sim R^2$ until the ratio σ/R becomes sufficiently large. The effect is akin to surface tension dominating the local force balance of fluid interfaces at small length scales. In Figure 16, the dimensionless characteristic swelling time t/τ is displayed for various choices of $\sigma/R[[c_\gamma]]$. We note the slight deviation from $\tau \sim R^2$ for sufficiently large σ . In Figure 17, plots of the dimensionless difference $(U - u)/\Theta$ of the diffusion potential of the reservoir and the diffusion potential on the interface are shown for the same choices of $\sigma/R[[c_\gamma]]$ used in generating Figure 16. As σ is increased, so too does the variation in $U - u$. Although we observe some deviation from $\tau \sim R^2$ for these cases, the associated magnitude of σ appears artificially large.

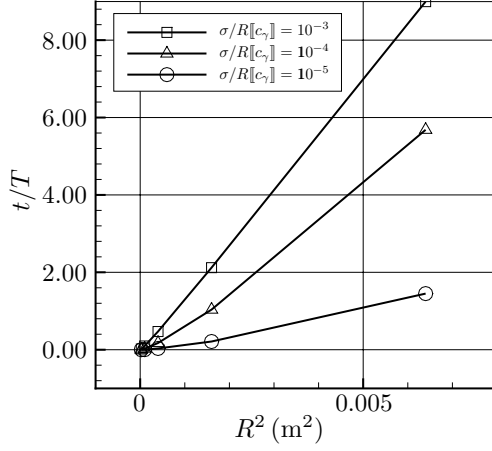


Figure 16: Characteristic swelling times as a function of initial gel radius squared for various σ .

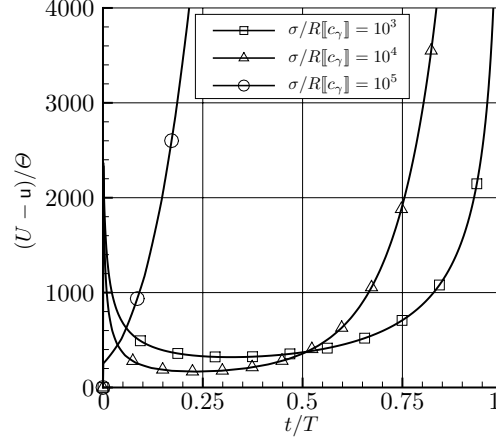


Figure 17: Diffusion potential difference as a function of time for various σ .

4.5.3 Hysteresis under cyclic loading

We now consider solutions to (4.21)–(4.31) with the initial and boundary conditions

$$s_0 = R, \quad U(t + T_*) = U(t), \quad (4.44)$$

corresponding to an initially collapsed specimen that is subjected to a cyclic variation, with period T_* , of the diffusion potential U of the reservoir. In particular, we discuss the response to a sawtooth cycle with amplitude Θ_* and minimum U_0 (Figure 18).

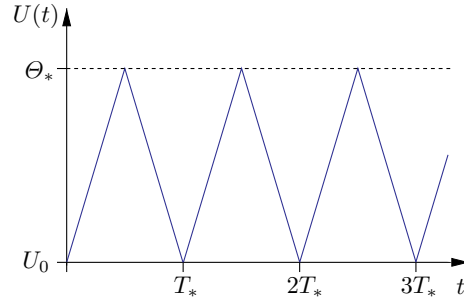


Figure 18: Excitation of diffusion potential on gel surface with period T and height Θ .

As U oscillates between U_c and U_{th} , our model predicts a hysteretic response in the swelling ratio Q . To illustrate this, we consider the case where the minimum diffusion potential of the reservoir is given by $U_0 = U_c + 0.40(U_{th} - U_c)$, $\Theta = 0.75(U_{th} - U_c)$, and $T_* = \tau/10$. The swelling ratio Q is plotted against U in Figure 19. Subsequent to an initial transient, the material response enters a limit cycle. Figure 20 compares the diffusion potential on the boundary to that of the interface. The situation $U > u$ corresponds to increasing Q and similarly $U < u$ to decreasing Q . We note that although the diffusion potential of the reservoir exceeds the threshold U_{th} , the period T_* of the cycle is not large enough to trigger total swelling. From Figure 20, it appears that the minimum of the diffusion potential u on the interface is shifted away from that of the

reservoir. In other words, there is a short interval of time during which U is increasing with time while u is still decreasing. During this interval the interface is still moving toward the boundary of the specimen, because $U < u$.

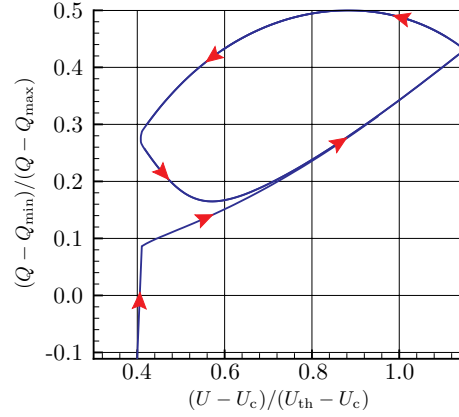


Figure 19: Swelling ratio vs. reservoir potential. Arrows indicate the direction of increasing time.

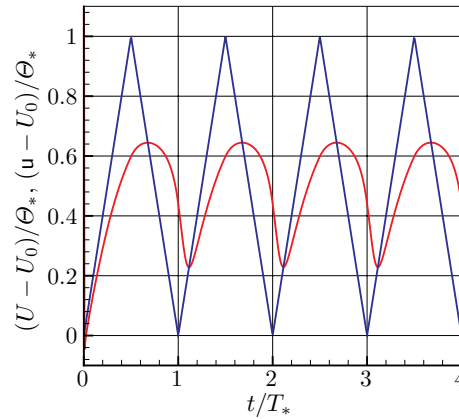


Figure 20: Temporal variations of the diffusion potential of the reservoir and the diffusion potential on the interface.

5 Summary and concluding remarks

With the emergence of technologies that rely on the novel swelling behavior of hydrogels comes a convincing need for physically accurate theories and numerical simulations capable of capturing analyzing and predicting this behavior. To design micro-actuation and sensing devices based on hydrogels, for example, predictions of swelling times and available force densities will be critical. By the same token, purely phenomenological or empirical models do not provide sufficient physical links to the various processes associated with the swelling of hydrogels. Without such links, the performance characteristics of the gels cannot be “optimized” during fabrication.

Motivated by the experimental observations of Gehrke et al. (1992), which suggest that swelling transitions proceed at a rate much slower than bulk diffusion, we work with a system of model equations in which the coupling between the deformation and solute concentration is solely through the interfacial normal configurational force balance. We recast this system in an equivalent, hybrid variational form, with the interfacial solute balance viewed within the framework of the level-set method. We describe suitable approximations for the deformation and diffusion potential in the context of the eXtended-Finite-Element/Level-Set Method (XFE/LSM). In particular, local enrichment functions are employed to capture the discontinuities in the gradients of the primary fields at the interface.

To illustrate some features of the governing equations and their numerical approximation, the swelling of a spherical specimen is studied. We consider a specimen whose boundary is traction-free and is in contact with a reservoir of uniform chemical potential. To capture the dramatic volume changes associated with swelling and collapse, we rely on strain-energy functions which depend on the energetically preferred dilatation for each phase. A series of parametric studies indicate good qualitative agreement with experimental observations. Most notably, we predict characteristic swelling times that are proportional to the square of the initial gel radius for a wide range of material properties. Previous models that gave this result are based upon the assumption of collective diffusion, which assumes that swelling occurs spontaneously throughout the material. In view of the major differences between the equations of the sharp-interface model and those of arising from the model based on collective diffusion, it seems likely that the quadratic dependence of swelling time upon specimen radius may reflect an underlying scaling law. It might be useful to explore the existence of such a law. In addition to our parametric studies, we also simulations involving cyclic variations of the diffusion potential of the reservoir; these simulations show that the swelling ratio exhibits hysteresis during such cycles.

From the perspective of materials design, several key conclusions can be extracted from our results. In particular, the results suggest that the response time for swelling can be decreased in at least three ways:

- (i) by designing the underlying polymer network so that the preferred dilatation J_α in the swelled phase is as large as possible;
- (ii) by increasing the mobility of the polymer chains in the swelled phase; and
- (iii) by adjusting the solvent such that the jump $\llbracket c_\gamma \rrbracket$ in polymer concentration between swelled and collapsed phases is maximized.

Obviously, a number of the above properties may not be independent, and only a detailed comparison with careful experiments will reveal the fidelity of our predictions.

We also remark that many stimulus-responsive gels swell in response to changes in pH or temperature and that our framework could easily be extended to account for these effects.

As a caveat to the foregoing remarks, we emphasize that the assumption that the time scale for swelling is much slower than that for bulk diffusion and the particular constitutive equations that we use may limit the applicability of our model. Further studies are necessary to determine the extent and nature of any such limitations.

Furthermore, our treatment of the boundary conditions for the gel surface neglects effects such as surface tension and the exchange of material, effects which may underlie the formation of wrinkles and other observed surface patterns. Extension of the theory to account for such effects and numerical studies of two-dimensional problems is therefore necessary.

References

- Armero, F. and K. Garikipati (1996). An analysis of strong discontinuities in multiplicative finite strain plasticity and their relation with the numerical simulation of strain localization in solids. *International Journal of Solids and Structures* 33, 2863–2885.
- Armero, F. and J. C. Simo (1992). A new unconditionally stable fractional step method for non-linear coupled thermomechanical problems. *International Journal for Numerical Methods in Engineering* 35, 737–766.
- Bai, G. and A. Suzuki (2000). Shrinking patterns and phase coexistence of polymer gels. *Materials and Design* 21, 547–550.
- Barriere, B. and L. Leibler (2003). Kinetics of solvent absorption and permeation through a highly swellable elastomeric network. *Journal of Polymer Science: Part B: Polymer Physics* 41, 166–182.
- Beebe, D. J., J. S. Moore, J. M. Bauer, Q. Yu, R. H. Liu, C. Devadoss, and B. Jo (2000). Functional hydrogel structures for autonomous flow control inside microfluidic channels. *Nature* 404, 588–590.
- Brooks, A. N. and T. J. R. Hughes (1982). Streamline upwind/Petrov-Galerkin formulations for convection dominated flows with particular emphasis on the incompressible Navier-Stokes equations. *Computer Methods in Applied Mechanics and Engineering* 32, 199.
- Budtova, T. (1998). Absorption/release of polyvalent metal ions by a polyelectrolyte gel. *Journal of Controlled Release* 54(3), 305–312.
- Budtova, T. and P. Navard (1998). Swelling kinetics of polyelectrolyte gel in water and salt solutions. Coexistence of swollen and collapsed phases. *Macromolecules* 31(25), 8845–8850.
- Chopp, D. L. (2001). Some improvements of the fast marching method. *SIAM Journal on Scientific Computing* 23(1), 230–244.
- Dolbow, J. (1999). *An extended finite element method with discontinuous enrichment for applied mechanics*. Ph. D. thesis, Northwestern University.
- Dolbow, J., N. Moës, and T. Belytschko (2000). Discontinuous enrichment in finite elements with a partition of unity method. *Finite Elements in Analysis and Design* 36, 235–260.
- Dolbow, J. E., N. Moës, and T. Belytschko (2001). An extended finite element method for modeling crack growth with frictional contact. *Computer Methods in Applied Mechanics and Engineering* 190, 6825–6846.
- Dušek, K. (Ed.) (1993). *Responsive Gels: Volume Transitions I, Advances in Polymer Science*, Volume 109, Berlin. Springer.
- Eichenbaum, G. M., P. F. Kiser, D. Shah, S. A. Simon, and D. Needham (1999). Investigation of the swelling response and drug loading of ionic microgels: The dependence on functional group composition. *Macromolecules* 32, 8996–9006.
- Garikipati, K. and V. S. Rao (2001). Recent advances in models for thermal oxidation of silicon. *Journal of Computational Physics* 174(1), 138–170.
- Gehrke, S. H., G. Agrawal, and M. C. Yang (1992). Moving ion exchange fronts in polyelectrolyte gels. *ACS Symposium Series* 480, 211–237.
- Gibbs, J. W. (1878). On the equilibrium of heterogeneous substances. *Transactions of the Connecticut Academy of Arts and Sciences* 3, 108–248.
- Gurtin, M. E. (1995). The nature of configurational forces. *Archive for Rational Mechanics and Analysis* 131(1), 67–100.
- Gurtin, M. E. (2000). *Configurational Forces as Basic Concepts in Continuum Physics*. New York: Springer.
- Gurtin, M. E. and A. Struthers (1990). Evolving phase boundaries in the presence of bulk deformation. *Archive for Rational Mechanics and Analysis* 112, 97–160.
- Gurtin, M. E. and P. W. Voorhees (1993). The continuum mechanics of coherent two-phase elastic solids with mass transport. *Proceedings of the Royal Society of London Series A* 440(1909), 323–343.
- Hughes, T. J. R. (1995). Multiscale phenomena - Green’s functions, the Dirichlet to Neumann formulation, subgrid scale models, bubbles and the origins of stabilized methods. *Computer Methods in Applied Mechanics and Engineering* 127(1–4), 387–401.

- Ji, H. (2001). A note on enrichment functions for gradient discontinuities. Technical Report 1, Department of Civil Engineering, Duke University.
- Ji, H., D. Chopp, and J. E. Dolbow (2002). A hybrid extended finite element/ level set method for modeling phase transformations. *International Journal for Numerical Methods in Engineering* 54, 1209–1233.
- Jirasek, M. (2000). Comparative study on finite elements with embedded discontinuities. *Computer Methods in Applied Mechanics and Engineering* 188(1–3), 307–330.
- Krongauz, Y. and T. Belytschko (1998). EFG approximation with discontinuous derivatives. *International Journal for Numerical Methods in Engineering* 41(7), 1215–1233.
- Lynch, D. R. and K. O’Neill (1981). Continuously deforming finite elements for the solution of parabolic problems, with and without phase change. *International Journal for Numerical Methods in Engineering* 17, 81–96.
- Matsuo, E. and T. Tanaka (1989). Kinetics of discontinuous volume phase-transition of gels. *Journal of Chemical Physics* 89(3), 1695–1703.
- Melenk, J. M. and I. Babuška (1996). The partition of unity finite element method: Basic theory and applications. *Computer Methods in Applied Mechanics and Engineering* 139, 289–314.
- Merle, R. and J. E. Dolbow (2002). Solving thermal and phase change problems with the extended finite element method. *Computational Mechanics* 28, 339–350.
- Moës, N., J. Dolbow, and T. Belytschko (1999). A finite element method for crack growth without remeshing. *International Journal for Numerical Methods in Engineering* 46, 131–150.
- Mullins, W. and R. Sekerka (1963). Morphological stability of a particle growing by diffusion and heat flow. *Journal of Applied Physics* 34, 323–329.
- Olsen, M., J. M. Bauer, and D. Beebe (2000). Particle imaging techniques for measuring the deformation rate of hydrogel microstructures. *Applied Physics Letters* 76(22), 3310–3312.
- Onuki, A. (1993). Theory of phase transition in polymer gels. In K. Dušek (Ed.), *Responsive Gels: Volume Transitions I, Advances in Polymer Science*, Volume 109, Berlin, pp. 63–121. Springer.
- Osher, S. and J. Sethian (1988). Fronts propagating with curvature dependent speed: Algorithms based on Hamilton-Jacobi formulation. *Journal of Computational Physics* 79, 12–49.
- Rao, V. S., T. J. R. Hughes, and K. Garikipati (2000). On modeling thermal oxidation of silicon II: numerical aspects. *International Journal for Numerical Methods in Engineering* 47, 359–377.
- Sethian, J. (1999). *Level Set Methods and Fast Marching Methods*. New York, NY: Cambridge University Press.
- Sukumar, N., D. L. Chopp, N. Moës, and T. Belytschko (2001). Modeling holes and inclusions by level sets in the extended finite element method. *Computer Methods in Applied Mechanics and Engineering* 190, 6183–6200.
- Tanaka, T. (1978). Collapse of gels and critical endpoint. *Physical Review Letters* 40(12), 820–823.
- Tanaka, T., L. Hocker, and G. B. Benedek (1973). Spectrum of light scattered from a viscoelastic gel. *Journal of Chemical Physics* 59, 5151–5159.
- Tanaka, T., E. Sato, Y. Hirokawa, S. Hirotsu, and J. Peetermans (1985). Critical kinetics of volume phase-transitions of gels. *Physical Review Letters* 55(22), 2455–2458.
- Tanaka, T., S. T. Sun, Y. Hirokawa, S. Katayama, J. Kucera, Y. Hirose, and T. Amiya (1987). Mechanical instability of gels at the phase transition. *Nature* 325(6107), 796–798.
- Tomari, T. and M. Doi (1994). Swelling dynamics of a gel undergoing volume transitions. *Journal of the Physical Society of Japan* 63(6), 2093–2101.
- Tomari, T. and M. Doi (1995). Hysteresis and incubation in the dynamics of volume transition of spherical gels. *Macromolecules* 28, 8334–8343.
- Udaykumar, H. S., R. Mittal, and W. Shyy (1999). Computation of solid-liquid phase fronts in the sharp interface limit on fixed grids. *Journal of Computational Physics* 153, 535–574.
- Zienkiewicz, O. C., D. K. Paul, and A. H. C. Chan (1988). Unconditionally stable staggered solution procedure for soil-pore fluid interaction problems. *International Journal for Numerical Methods in Engineering* 26, 1039–1055.